Available online at www.sciencedirect.com
ScienceDirect
Journal of Solid State Chemistry 179 (2006) 3607–3614
JOURNAL OF SOLID STATE CHEMISTRY
www.elsevier.com/locate/jssc

# The low-temperature form of $Rb_2KCrF_6$ and $Rb_2KGaF_6$: The first example of an elpasolite-derived structure with pentagonal bipyramid in the B-sublattice

Francisco Javier Zúñiga[a], Alain Tressaud[b,*], Jacques Darriet[b]

[a]*Departamento de Fisica de la Materia Condensada, Facultad de Ciencia y Tecnología, Universidad del Pais Vasco, Apdo 644, 48080 Bilbao, Spain*
[b]*Institut de Chimie de la Matière Condensée de Bordeaux (ICMCB, UPR 9048 CNRS), Université de Bordeaux 1, 87 avenue du Docteur Albert Schweitzer, 33608 Pessac Cedex France*

Received 2 June 2006; received in revised form 19 July 2006; accepted 22 July 2006
Available online 27 July 2006

**Abstract**

The crystal structure of the low-temperature forms of $Rb_2KCrF_6$ and $Rb_2KGaF_6$ has been solved on single crystal. The symmetry is tetragonal with $F4/m$ space group; the unit cell parameters are: $a = 19.407(3)$ Å, $c = 8.833(2)$ Å for $Rb_2KCrF_6$ at $T = 90$ K and $a = 19.375(4)$ Å, $c = 8.782(2)$ Å for $Rb_2KGaF_6$ at $T = 90$ K. The relationships between the parameters of the prototype cubic elpasolite, which is stable at high temperature, and the tetragonal superlattice of the low temperature form have been established. Considering the general formulation $A_2BB'F_6$, the cationic positions in the $A$ and ($B$,$B'$) sublattices remain identical in the two allotropic varieties. The main originality of the structure concerns the environment of 4/5 of the potassium atoms ($B$ sublattice) which is transformed from octahedra into pentagonal bipyramids sharing edges with adjacent $B'F_6$ octahedra containing Cr or Ga. The displacive phase transition is simply explained by the rotation of 45° in the ($a$,$b$) plane of 1/5 of the $B'F_6$ ($B'$ = Cr, Ga) octahedra. The similarity of this phase transition and the transformation of perovskite into tetragonal tungsten bronze (TTB) will be discussed.


*Keywords:* Perovskite-derived; Elpasolite; Complex fluorides; Structural phase transitions; Pentagonal bipyramid environment

## 1. Introduction

The perovskite structure constitutes one of the most important prototypes in solid-state chemistry, both from fundamental and applied viewpoints, i.e. ferroelectricity, luminescence, high $T_C$ superconductors, etc. The structure, which corresponds the general $ABX_3$ formula ($Pm$-3$m$ cubic symmetry), is formed of $BX_6$ octahedra 3-D connected through corners, whereas $A$ cations are located in the central site with coordination number CN = 12. Elpasolite $A_2BB'X_6$ and cryolite $A_3BX_6$ types derive from the perovskite by a cationic ordering ($Fm$-3$m$ cubic symmetry). Unlike in simple perovskites in which all octahedra are equivalent, in elpasolites two types of $BX_6$ and $B'X_6$ octahedra alternate along the three directions. Many fluorides with general $A_2BMF_6$ formula, with $M$ = trivalent cation crystallize with the elpasolite type [1,2].

In many of these compounds, structural phase transitions (SPT) have been shown to occur in a large temperature range, depending on the value of the steric tolerance factor $t$ [3]. The size of the involved cations is decisive and affects considerably the sequence and the stability range of the low-temperature distorted phases. Such point can be illustrated by the rare-earth based $Rb_2KMF_6$ series. For smallest ionic radii: $M$ = Lu, Sc or In, two successive SPTs are observed from high to low temperatures: $Fm$-3$m \rightarrow I4/m \rightarrow P21/n$. The stability range of the intermediate tetragonal phase decreases with increasing size of $M^{3+}$ cation and for $r\ M^{3+} > 0.88$ Å, that is for $M$ = Ho, Dy, Tb, only one structural transition is observed: $Fm$-3$m \rightarrow P21/n$ [4]. In these phases, SPTs can be connected with small octahedral tilts around one (two or

*Corresponding author. Fax: +33 5 40 00 27 61.
*E-mail address:* tressaud@icmcb-bordeaux.cnrs.fr (A. Tressaud).

0022-4596/$ - see front matter © 2006 Elsevier Inc. All rights reserved.
doi:10.1016/j.jssc.2006.07.032

Table 1
Structural phase transitions in $Rb_2KMF_6$ elpasolites [from 6]

| $Rb_2KMF_6$ | $rM^{3+}$ [5] | $t$ [3] | Cubic unit-cell (Å) at 300 K | SPT (K) |
|---|---|---|---|---|
| Al | 0.53 | 0.89 | 8.68 | No, down to 77 K |
| Cr | 0.615 | 0.88 | 8.81 | 153 |
| Fe | 0.645 | 0.87 | 8.87 | 170 |
| Ga | 0.62 | 0.875 | 8.80 | 123 |

three) of the fourfold axes of the cubic phase, and subsequently, the total entropy could be calculated by summarizing the entropies of the successive tilts [4].

In the case of smaller $M^{3+}$, that is for $d$ transition element or similar cations, the exact symmetry of the low-temperature phase has not been elucidated, so far [2]. $Rb_2KMF_6$ fluorides, with $M$ = Cr, Fe, Ga, exhibit at room temperature the cubic prototype structure and undergo a SPT below room temperature (Table 1) with a lowering of symmetry. In the previous studies, the low-temperature X-ray diffraction patterns were generally indexed in a pseudo-tetragonal symmetry, with unit cell constants equal to $a_{tetrag} = a_{cub}/\sqrt{2}$, $c_{tetrag} = a_{cub}$ [6–8]. The sequence of ferroelastic phase transitions in $Rb_2KFeF_6$ and $Rb_2KGaF_6$ were compared with the ones found for larger trivalent cations: rare-earths, Sc, In [9] and the dependence of the thermodynamical characteristics were studied in the $Rb_2KGa_xSc_{1-x}F_6$ solid solutions [10]. A luminescence study of $Cr^{3+}$-doped $Rb_2KGaF_6$ confirmed that the octahedral fluoro-environment of chromium was maintained in the low-temperature phase below the first-order transition at around 125 K, which exhibited a hysteresis phenomenon [11].

In spite of all these studies, the real symmetry of the low-temperature phase of $Rb_2KMF_6$, $M$ = Cr, Ga and the corresponding SPT mechanisms remained to be elucidated [12]. This is the subject of the present paper.

## 2. Experimental

### 2.1. Synthesis and single crystals

Powdered samples of $Rb_2KCrF_6$ and $Rb_2KGaF_6$ were synthesized by solid-state reaction from stoichiometric mixtures of compositions: $2RbF + KF + MF_3$. Due to their hygroscopicity, the starting fluorides were handled in a glovebox. The reactions were carried out at 700 °C in sealed gold tubes and followed by quenching. The colors of the compounds are green and white, respectively. Single crystals were obtained in a sealed platinum crucible using the Bridgman method. After being heated 50 °C above the melting temperature for 10 h, the crucible was moved down to the cooler part of the furnace with a thermal gradient of 2.5 K/mm at 1.5 mm/h.

### 2.2. Crystal data, symmetry and twin components

Samples for X-ray diffraction were obtained by selecting small pieces from good optical quality crystals. Single crystal X-ray diffraction data from $Rb_2KCrF_6$ and $Rb_2KGaF_6$ samples were collected with an Xcalibur (Oxford Diffraction) diffractometer with CCD area detector, with sealed-tube Mo$K\alpha$ X-ray source. For measurements at low temperature, an open flow cryostat (Oxford Cryosystem) was used. Data collections were carried out at room temperature for the prototype high-temperature phase and at 90 K in the low-temperature phase. The reported transition temperatures for the Ga and Cr-compounds were $T$ = 123 and 153 K, respectively [2,6,10]. Experimental details relative to the three structural determinations reported in this paper are summarized in Table 2. Integration of intensities and data reduction applied to the different data sets were performed using the CrysAlis Software Package [13] . The program package Jana2000 [14] was used for the numerical absorption correction and structure refinements.

At room temperature, the diffraction data from both compounds could be interpreted with the face centered cubic elpasolite unit cell with $a_c \sim 8.8$ Å (see lattice parameters in Table 2). The precession diffraction sections reconstructed from the collected frames show extinction conditions and reciprocal space symmetry compatible with the $Fm$-3$m$ space group, this symmetry corresponding to the prototype elpasolite cubic phase.

After completing the room temperature data collection, crystals were cooled down to 90 K at a rate of 60 K/min. Temperature stability during data collection was kept within $\pm 0.2$ K. In both compounds, the reconstructed precession diffraction patterns show that, in addition to the set of reflections belonging to the room temperature elpasolite cubic cell, the reciprocal space contains a new set of weak superlattice reflections. These reflections, together with those defining the elpasolite sublattice, show an overall 4/$m$ tetragonal symmetry and could be fully indexed in a twinned face-centered tetragonal superlattice with $a = 2a_c + b_c$, $b = -a_c + 2b_c$ and $c = c_c$. The reflection conditions are compatible with the unconventional $F4/m$ space group related to the $I4/m$ space group (87). The elpasolite sub-cell parameters at 90 K are $a = 8.687(4)$ Å, $b = 8.670(3)$ Å and $c = 8.740(3)$ Å for the Ga-compound and $a = 8.689(2)$ Å, $b = 8.682(2)$ Å and $c = 8.822(2)$ Å for the Cr compound, with $c/a$ ratios of 1.007 and 1.016, respectively. Comparing these values with those of the room temperature phase (8.807(2) and 8.817(3) Å for the Ga and Cr-compounds, respectively), the transition involves lattice distortions along the $a$ and $c$-axis of 1.45% and 0.8% for the Ga-compound, and 1.49% and −0.06% for the Cr-compound (negative value means a negative dilatation). The lengths of tetragonal super-cell axis refined without any metric constrain are $a = 19.373(4)$ Å, $b = 19.376(4)$ Å and $c = 8.782(2)$ Å for the Ga-compound and 19.411(3) Å, $b = 19.402(3)$ Å and $c = 8.833(2)$ Å for the

Table 2
Crystal data and structural refinement for $Rb_2KGaF_6$ and $Rb_2KCrF_6$

| | | | |
|---|---|---|---|
| Formula | $Rb_2KGaF_6$ | | $Rb_2KCrF_6$ |
| Crystal color | Transparent | | Green |
| $M_w$ (g mol$^{-1}$) | 393.7 | | 376.0 |
| Temperature (K) | 293 | $90\pm0.2$ | $90\pm0.2$ |
| Space group | *Fm*-3*m* | *F*4/*m* | *F*4/*m* |
| Parameters (*a*, *c*) | 8.807(2) | 19.375(4), 8.782(2) | 19.407(3), 8.833(2) |
| *V* (Å$^3$) | 683.1(3) | 3296.7(12) | 3326:8(10) |
| *Z* | 4 | 20 | 20 |
| Dx. (g cm$^{-3}$) | 3.827 | 3.965 | 3.753 |
| Crystal size (mm) | | | |
| Diffractometer | | Xcalibur CCD | |
| Radiation | | Mo*K*α | |
| Scan mode | | ω and φ-scans | |
| h k l range | $-13/6\pm13$, $\pm12$ | $-28/17$, $\pm28$, $\pm12$ | $\pm36$, $\pm37$, $\pm17$ |
| $\theta_{min}/\theta_{max}$ | 4/32 | 2.8/32 | 2.8/44.5 |
| μ (cm-1) | 18.831 | 19.51 | 16.92 |
| Absorption correction | | Gaussian | |
| $T_{min}/T_{max}$ | 0.2192/0.6480 | 0.2242/ 0.5504 | 0.2209/ 0.4303 |
| No of reflections | 3011 | 7671 | 20287 |
| $R_{int}$ | 0.051 | 0.0771 | 0.0749 |
| No of independent reflections | 86 | 1450 | 1743 |
| Reflections with $I>3\sigma$ (*I*) | 79 | 453 | 1342 |
| Refinement | | *F* | |
| *F*(000) | 712 | 3560 | 3420 |
| *R*(obs/all) | 0.0372/0.0446 | 0.0375/0.129 | 0.0615/0.0797 |
| $R_w$ (obs/all) | 0.0207/0.0209 | 0.0293/0.0375 | 0.0666/0.0709 |
| No. of refined parameters | 8 | 73 | 73 |
| g.o.f.(obs) | 4.70 | 1.83 | 2.41 |
| Weighting scheme | | $1/\sigma^2(I)$ | |
| Δρ (max/min) (e$^-$/Å$^3$) | 2.60/−4.75 | 2.61/−2.64 | 3.57/−3.89 |

Cr-compound (see Table 2 for lattice parameters with metric restriction). The room temperature elpasolite cubic cell and the low temperature tetragonal cell are outlined in Fig. 1.

As above-mentioned, the diffraction patterns could be only fully interpreted as due to twinned crystals. The transition from the cubic to tetragonal symmetry introduces as many orientation domains as rotation and mirror symmetry elements are lost in the transition. In this case, it can be expected that crystal in the low temperature form exhibits up to six domains related by the four-fold, three-fold and mirror planes symmetry elements lost when reducing the symmetry from *m*-3*m* to 4/*m*. Matrixes in the cubic base relating domains are unitary, but when expressed in the tetragonal base they take the values

$$\begin{pmatrix}1&0&0\\0&1&0\\0&0&1\end{pmatrix}\quad\begin{pmatrix}3/5&-4/5&0\\-4/5&-3/5&0\\0&0&-1\end{pmatrix}\quad\begin{pmatrix}1/5&2/5&2/5\\2/5&4/5&-1/5\\-2&1&0\end{pmatrix}$$
$$\begin{pmatrix}1/5&2/5&-2/5\\2/5&4/5&1/5\\2&-1&0\end{pmatrix}\quad\begin{pmatrix}4/5&-2/5&1/5\\-2/5&1/5&2/5\\-1&-2&0\end{pmatrix}\quad\begin{pmatrix}4/5&-2/5&-1/5\\-2/5&1/5&-2/5\\1&2&0\end{pmatrix}.$$

Note that, owing to the small tetragonal distortion that undergoes the cubic room-temperature cell at low temperature, the elpasolite cubic reciprocal lattice vectors of all twin components almost coincide, and the integrated intensities of these diffraction vectors contain the contribution of all domains. This is not the case for the superlattice reflection defining the large tetragonal cell, since the associated reciprocal lattice vectors of the different twins have different orientations. This fact was

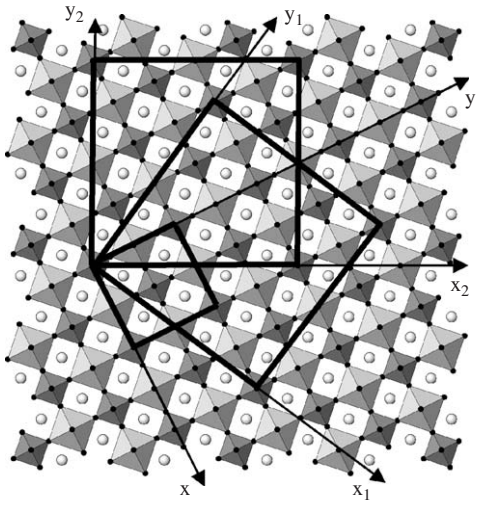


Fig. 1. Projection of the prototype elpasolite structure along the [001] direction. Heavy line outlines the room temperature cubic cell. Gray line outlines the tetragonal *F*4/*m* low temperature cell of two domains ($X_1Y_1$) and ($X_2Y_2$) related by a mirror plane perpendicular to the [100] cubic direction.

taken into account in the next refinement step and the above given matrixes were used to calculate the contribution of the different domains to each integrated intensity.

### 2.3. Refinements

The room temperature structure of $Rb_2KGaF_6$ was refined assuming the symmetry space group *Fm*-3*m* and using as starting parameters those reported for Cr compound by Siebert et al. [15]. The refinement based on F including anisotropic thermal displacements converges down to $R = 0.037$ in a few cycles (Table 2). The structural parameters are gathered in Table 3.

For the refinements of the low temperature phases, an initial structural model was first created spanning the cubic room temperature atomic positions over the tetragonal supercell. The twinned domains related by the above matrixes were taken into account and their relative volumes included in the refinement process. Those fractional volumes taking values close to zero or becoming negative were fixed to 0 during the refinement (one value in the Ga-compound and two for the Cr-compound). Using anisotropic displacement parameter for all positions, the residual factor converged to values given in Table 2 and the difference-Fourier residues were reduced to a non-significant noise, except on the K-positions. The final atomic site parameters are given in Tables 4 and 5 with interatomic distances in Table 6.

Recently, it has been proposed that an orthorhombic distorted ($\gamma$) phase ($a = 3a_c - 3c_c$, $b = 2b_c$, $c = a_c + c_c$, *Fddd* space group), appears within a complex phase transition sequence in the related compound $K_3AlF_6$ below the Fm3m high temperature form [16]. The reported electron diffraction patterns showed similarities with the X-ray patterns observed for our compounds which could be also indexed using the orthorhombic cell. Such a structural model has been tested in the case of the Ga-compound by refining the structure with the *Fddd* space group. The results lead to worse *R*-factor values of 0.071 and 0.29 for the observed and all reflection, respectively, which allowed us to discard this hypothesis with orthorhombic symmetry.

## 3. Results and discussion

A view of the ambient- and the low-temperature structures is given in Fig. 2. It should be noted that the cationic ordering is absolutely identical to that encountered in the room temperature cubic form of the elpasolite (compare Figs. 2a and b). The rubidium atoms occupy the *A*-sites and the potassium atoms and the chromium (or gallium) atoms are distributed with an order 1-1 in the *B* and *B*′ sites of the elpasolite having the general formulation $A_2BB'F_6$. The lowering of symmetry of cubic to tetragonal observed according to the temperature implies a doubling of each independent sites *B* and *B*′ (Tables 4 and 5). The most important structural difference between the two allotropic forms of the $Rb_2KMF_6$ ($M$ = Cr, Ga) fluorides is the change of coordination number of the potassium atoms occupying the K2 sites (Tables 4 and 5). The coordination number becomes equal to 7 with a bipyramidal pentagonal type environment (Fig. 2b). The K–F interatomic distances within this polyhedron range between 2.514 and 2.834 Å for the Cr-phase and between the two limits of 2.51 and 2.87 Å for the Ga-phase (Table 6). The calculation of the bond valence sum (BVS) using the basis of the data of Brese and O' Keefe [17] leads to the values of 1.21(1) (Cr) and 1.22(2) (Ga). These values are in good agreement with the expected value for potassium ion.

Table 3
Structural parameters of cubic F*m*-3*m* $Rb_2KGaF_6$ at room temperature

| Atoms | Atomic positions | *x* | *y* | *Z* | $U_{eq}$ (Å)$^2$ |
|---|---|---|---|---|---|
| Ga | 4a | 0 | 0 | 0 | 0.0122(3) |
| Rb | 8c | 1/4 | 1/4 | ¼ | 0.0264(3) |
| K | 4b | 1/2 | 1/2 | ½ | 0.0129(6) |
| F | 24e | 0.2148(5) | 0 | 0 | 0.0390(15) |

Table 4
Structural parameters of tetragonal $Rb_2KGaF_6$ at 90 K

| Atom | *x* | *y* | *Z* | $U_{eq}$ (Å)$^2$ |
|---|---|---|---|---|
| Rb1 | 1/4 | 1/4 | ¼ | 0.0094(7) |
| Rb2 | 0.15924(8) | 0.05298(10) | 0.2727(2) | 0.0138(5) |
| K1 | 0 | 0 | ½ | 0.011(2)) |
| K2 | 0.32147(18) | 0.0890(2) | 1/2 | 0.0106(11) |
| Ga1 | 0 | 0 | 0 | 0.0143(16) |
| Ga2 | 0.30044(16) | 0.10450(15) | 0 | 0.0093(8) |
| F1 | 0.0943(5) | 0.0295(6) | 0 | 0.016(2) |
| F2 | 0 | 0 | 0.218(2) | 0.024(5) |
| F3 | 0.3873(5) | 0.0612(6) | 0 | 0.009(3) |
| F4 | 0.3449(6) | 0.1902(5) | 0 | 0.009(3) |
| F5 | 0.2145(6) | 0.1474(6) | 0 | 0.009(3) |
| F6 | 0.2580(6) | 0.0157(5) | 0 | 0.008(3) |
| F7 | 0.3019(5) | 0.1022(5) | 0.2161(9) | 0.024(2) |

Table 5
Structural parameters of tetragonal $Rb_2KCrF_6$ at 90 K

| Atom | *x* | *y* | *z* | $U_{eq}$ (Å)$^2$ |
|---|---|---|---|---|
| Rb1 | 1/4 | 1/4 | 1/4 | 0.0082(5) |
| Rb2 | 0.15906(7) | 0.05303(7) | 0.2736(2) | 0.0097(4) |
| K1 | 0 | 0 | 1/2 | 0.006(1) |
| K2 | 0.3228(2) | 0.0891(2) | 1/2 | 0.012(1) |
| Cr1 | 0 | 0 | 0 | 0.012(1) |
| Cr2 | 0.3006(2) | 0.1041(2) | 0 | 0.0060(7) |
| F1 | 0.0946(5) | 0.0313(6) | 0 | 0.020(3) |
| F2 | 0 | 0 | 0.217(2) | 0.027(4) |
| F3 | 0.3880(6) | 0.0596(6) | 0 | 0.015(3) |
| F4 | 0.3468(5) | 0.1931(5) | 0 | 0.007(3) |
| F5 | 0.2152(6) | 0.1473(6) | 0 | 0.017(3) |
| F6 | 0.2569(5) | 0.0152(5) | 0 | 0.006(3) |
| F7 | 0.3017(4) | 0.1028(4) | 0.2159(6) | 0.013(2) |

Table 6
Interatomic distances in Å in the low temperature forms of $Rb_2KCrF_6$ and $Rb_2KGaF_6$

| Atom | Atom | $d$ (Å) (Cr) | $d$ (Å) (Ga) |
|---|---|---|---|
| Rb1 | F4 | 3.102(7) | 3.080(8) |
| | $F4^{i}$ | 3.102(7) | 3.080(8) |
| | $F4^{ii}$ | 3.102(7) | 3.080(8) |
| | $F4^{iii}$ | 3.102(7) | 3.080(8) |
| | F5 | 3.051(8) | 3.046(6) |
| | $F5^{i}$ | 3.051(8) | 3.046(6) |
| | $F5^{ii}$ | 3.051(8) | 3.046(6) |
| | $F5^{iii}$ | 3.051(8) | 3.046(6) |
| | F7 | 3.043(8) | 3.047(9) |
| | $F7^{iii}$ | 3.043(8) | 3.047(9) |
| | $F7^{iv}$ | 3.043(8) | 3.047(9) |
| | $F7^{v}$ | 3.043(8) | 3.047(9) |
| Rb2 | F1 | 2.753(5) | 2.750(5) |
| | $F3^{vi}$ | 3.100(9) | 3.12(1) |
| | $F3^{iii}$ | 3.007(9) | 2.983(9) |
| | $F4^{iii}$ | 2.866(7) | 2.877(9) |
| | F5 | 3.220(8) | 3.195(8) |
| | F6 | 3.160(7) | 3.150(8) |
| | $F6^{vi}$ | 2.901(7) | 2.880(9) |
| | F7 | 2.976(8) | 2.96(1) |
| | $F7^{vi}$ | 3.120(8) | 3.10(1) |
| | $F7^{iii}$ | 3.024(8) | 3.02(1) |
| K1 | F2 | 2.496(16) | 2.48(2) |
| | $F2^{vii}$ | 2.496(16) | 2.48(2) |
| | $F3^{viii}$ | 2.463(11) | 2.48(1) |
| | $F3^{vi}$ | 2.463(11) | 2.48(1) |
| | $F3^{ix}$ | 2.463(11) | 2.48(1) |
| | $F3^{iii}$ | 2.463(11) | 2.48(1) |
| K2 | $F1^{vi}$ | 2.834(12) | 2.83(1) |
| | $F1^{ii}$ | 2.833(13) | 2.87(1) |
| | $F4^{iii}$ | 2.807(11) | 2.84(1) |
| | $F5^{ii}$ | 2.514(12) | 2.51(1) |
| | $F6^{vi}$ | 2.550(10) | 2.55(1) |
| | F7 | 2.557(6) | 2.533(8) |
| | $F7^{x}$ | 2.557(6) | 2.533(8) |
| Cr1/Ga1 | F1 | 1.934(10) | 1.92(1) |
| | $F1^{xi}$ | 1.934(10) | 1.92(1) |
| | $F1^{xii}$ | 1.934(10) | 1.92(1) |
| | $F1^{xiii}$ | 1.934(10) | 1.92(1) |
| | F2 | 1.921(16) | 1.91(2) |
| | $F2^{xi}$ | 1.921(16) | 1.91(2) |
| Cr2/Ga2 | F3 | 1.903(12) | 1.89(1) |
| | F4 | 1.946(10) | 1.87(1) |
| | F5 | 1.857(12) | 1.85(1) |
| | F6 | 1.922(10) | 1.91(1) |
| | F7 | 1.907(5) | 1.901(8) |
| | $F7^{xiv}$ | 1.907(5) | 1.901(8) |

(i) $1/2-x$, $1/2-y$, $-z$; (ii) $1/2-y$, $x$, $1/2+z$; (iii) $y$, $1/2-x$, $1/2-z$; (iv) $1/2-x$, $1/2-y$, $z$; (v) $1/2-y$, $x$, $1/2-z$; (vi) $1/2-x$, $-y$, $1/2-z$; (vii) $-x$, $-y$, $1-z$; (viii) $-1/2+x$, $y$, $1/2+z$; (ix) $-y$, $-1/2+x$, $1/2+z$; (x) $x$, $y$, $1-z$; (xi) $-x$, $-y$, $-z$; (xii) $-y$, $x$, $z$; (xiii) $y$, $-x$, $-z$; (xiv) $x$, $y$, $-z$.

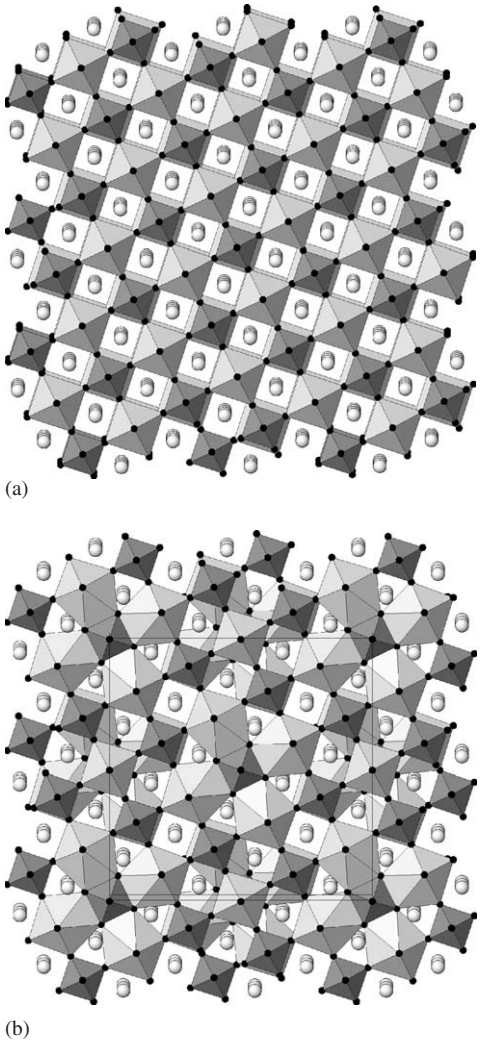

Fig. 2. View of the cubic $Rb_2KMF_6$ ($M$ = Cr, Ga) elpasolite-type structure (a) and tetragonal low temperature variety (b). The gray octahedra and pentagonal bipyramids correspond to $KF_6$ and $KF_7$ polyhedra. The $MF_6$ octahedra are smaller and darker shaded.

As shown in Fig. 2b, these pentagonal bipyramids are associated in the ($a$,$b$) plane by corner sharing (position F1) in order to constitute entities of four pyramids which generate in their center an octahedral site occupied by either chromium or gallium (positions Cr1 or Ga1, see Tables 3 and 4) (Fig. 2b). Four-fifth of the potassium atoms occupy the pentagonal sites whereas the remaining fifth is localized in the classical octahedral environment (K1 position, Tables 4 and 5). The K–F distances within the octahedral sites lie between 2.463 and 2.496 Å for the Cr phase, and is equal to 2.48 Å for the Ga phase (Table 6). It should be noted that the calculation of the BVS led in both cases to the values of 1.62(2) (Cr) and 1.60(2) (Ga) showing that this atom of potassium is over bonded. This structural constrain is surely at the origin of the structural transition observed at higher temperature for the two fluorides. Indeed for $Rb_2KGaF_6$ at room temperature, the BVS calculation for the potassium atoms leads to the smaller value of 1.47(2).

All the $M$ atoms ($M$ = Cr, Ga) are located in octahedra as in the cubic elpasolite (Table 6). The metal–fluorine distances are in good agreement with trivalent ions which is confirmed by the BVS calculations. The calculated values are 2.74(2) (position Cr1) and 2.92(2) (position Cr2) for the Cr-phase and 2.69(3) (Ga1) and 2.92(3) (Ga2) for the

Ga-phases. Finally, it is important to notice that a F–F minimum distance of 2.67(1) Å observed in $Rb_2KCrF_6$ and 2.63(1) Å in $Rb_2KGaF_6$ are in good agreement with those generally encountered in fluorides having non-bonded anion–anion separation.

The study of the structural distortions of the $ABX_3$ perovskite type-structure gave rise to many papers. The principle of the deformations is based on three variables defining the tilt angles of the $BX_6$ octahedra compared to its three principal axes. A classification was established according to the various possible types of rotation [18–21]. Indeed all rotations are not possible because the condition must be observed that all the $BX_6$ octahedra share corners in the three directions of the space. Tilting of octahedra must necessarily reduce the symmetry of the aristotype space group $Pm\text{-}3m$ and then generate derivative subgroups of lower symmetry [20,21].

The ideal 1:1 B-site ordered perovskites derive from the ideal cubic $ABX_3$ perovskite by an ordering of the B-cations along (1 1 1) planes. The general formula is written as $A_2BB'X_6$ to emphasize the two types of cations in octahedral coordination. These phases exhibit complete long-range order with no exchange of the $B$-site cations over the two available crystallographic sites and no tilting of $BX_6$ or $B'X_6$ octahedra. They crystallize in the space group $Fm\text{-}3m$ and have a cubic $2a_p$ unit cell. Numerous halides 1:1 ordered perovskites are known, of which the fluoro-perovskites of the elpasolite ($K_2NaAlF_6$) group are the most important. A section at $z = 0$ of the cubic elpasolite is given in Fig. 3a where one can see the ordering of the $B$ and $B'$ sublattice. As for the simple $ABX_3$ perovskite, the derived space groups for 1:1 ordered perovskites for all possible tilt systems can been deduced from Glazer classification [22]. The most common origin of displacive phase transition in the elpasolite-like fluorides, as well as in double perovskites are cooperative tilts of the $BF_6$ and $B'F_6$ octahedra in order to optimize the coordination environment of the $A$-cations and to preserve the three-dimensional framework of corners sharing octahedra. The superstructures observed for the low temperature variety of $Rb_2KCrF_6$ and $Rb_2KGaF_6$ are not among these possibilities proposed in [22]. In fact the transition from cubic elpasolite (Fig. 3a) to the tetragonal polymorph (Fig. 3c) does not imply cooperative tilts of all the octahedra. Indeed, the rotational mechanism concerns one-fifth only of the $MF_6$ octahedra (position Cr1 or Ga1 in Tables 4 and 5, respectively), which are surrounded by a circle in Fig. 3a. These octahedra undergo a rotation of 45° in the ($a$,$b$) plane, which is the maximum possible tilting angle in an octahedra. This rotation is limited to isolated octahedra and may explain why this type of lowering of the symmetry had not been imagined so far. The consequence is a drastic change of the coordination environment of the adjacent potassium atoms. The $KF_6$ octahedra observed in the cubic elpasolite are changed into pentagonal bipyramids sharing edges with the rotated $MF_6$ ($M$ = Cr, Ga) octahedra (Fig. 3c). An intermediary stage in the rotation

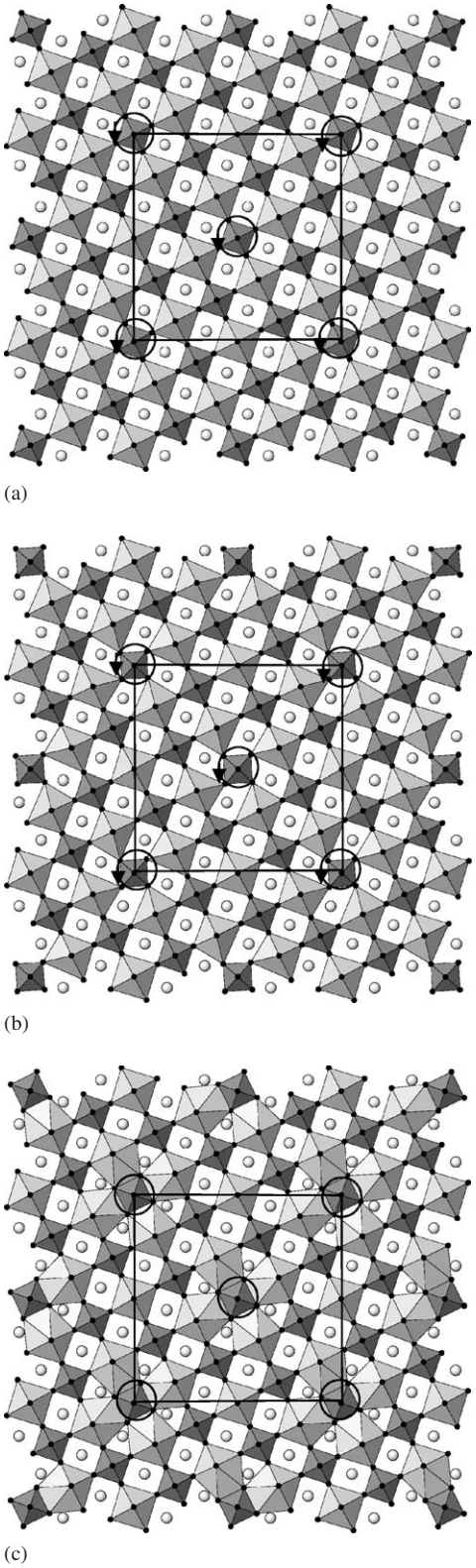


Fig. 3. Transformation of the cubic elpasolite (a) into the tetragonal low temperature variety of $Rb_2KMF_6$ ($M$ = Cr, Ga) (b) by a simple rotation of 45° in the ($a$,$b$) plane of the $MF_6$ octahedra surrounded by a circle. (c) An intermediate stage in the rotational mechanism where one can notice the deformation of the $KF_6$ octahedra which, in the final stage, are transformed into $KF_7$ polyhedra.

has been imagined to figure out the deformation of the polyhedra of the potassium atoms involved in this rotational mechanism (Fig. 3b).

This mechanism of 45° rotation is not without recalling the transformation of *A*-deficient perovskite into tetragonal tungsten bronze (TTB) as illustrated in Fig. 4 [23]. The TTB structure can be derived from the *A*-deficient perovskite (Fig. 4a) by cylindrical rotation faults, i.e. rotation of a square group of four corner-sharing octahedra through 45° (Fig. 4b). Some of the *A*-cuboctahedra sites are transformed into pentagonal prisms and empty tricapped trigonal prisms (Fig. 4b).

A similar phenomenon is observed in the tetragonal structures of $Rb_2KCrF_6$ and $Rb_2KGaF_6$ in which the environment of the rubidium atoms in Rb2 position is located at the center of a capped deformed triangular prism (Fig. 5b), whereas the rubidium atoms occupying the Rb1 position remain located within cuboctahedra as in cubic perovskite (Fig. 5a). The various Rb–F distances are gathered in Table 6.

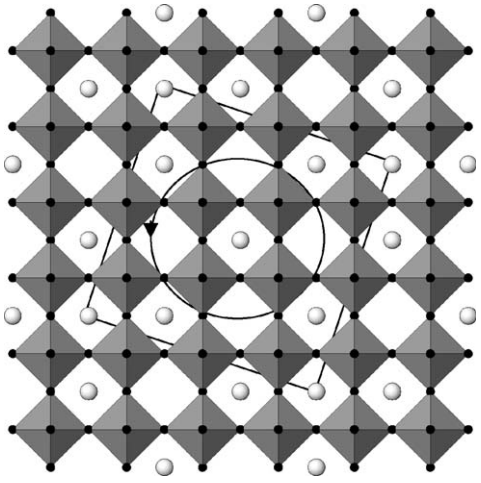

(a)

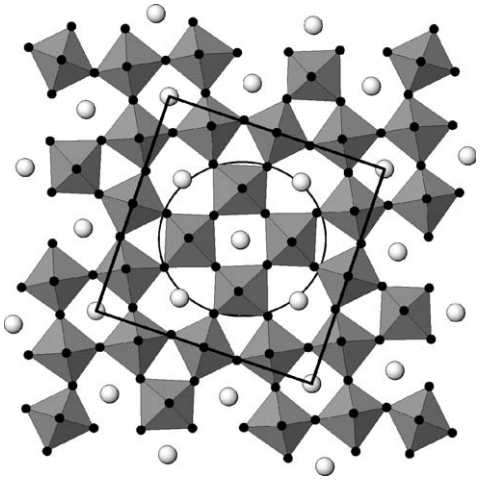

(b)

Fig. 4. TTB structure resulting from perovskite-like framework by a rotation of 45°. (a) Cubic perovskite with a deficit of 40% in the *A*-sites. The 'perovkiste' column involved in the rotation is surrounded by a circle. (b) Final step of the rotation of 45° of the column giving rise to the structure of TTB.

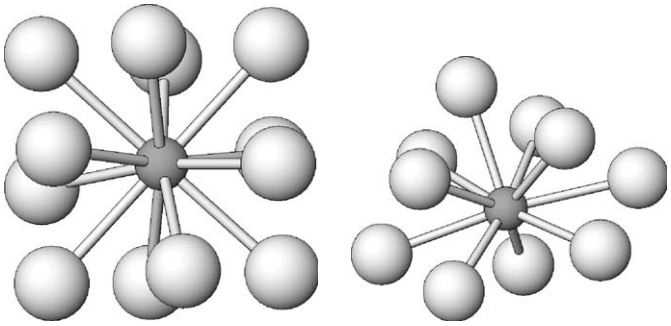

(a) (b)

Fig. 5. Environments of the rubidium atoms in the low temperature form of $Rb_2KCrF_6$ and $Rb_2KGaF_6$. (a) Rb1 position and (b) Rb2 position.

## 4. Conclusions

The crystal structure of the low temperature form of $Rb_2KCrF_6$ and $Rb_2KGaF_6$ has been determined for the first time. The cubic ↔ tetragonal phase transition does not involve change in the cationic repartition. The main difference is a strong deformation of the fluorine network which results in a drastic change in the environment of some potassium atoms. A simple mechanism based on the rotation of one fifth of the $MF_6$ octahedra is proposed to explain the phase transition. This new structural model does not belong to the known classification for the deformations in double perovskite because the proposed rotational mechanism is purely localized and not cooperative as it is required in the Glazer's classification. Such new structural type could be named as "*rotated-elpasolite*".

It is clear that the recent explanations given to interpret the phase transitions in $K_3MoO_3F_3$ [24] and in $K_3AlF_6$ [16] should be reinvestigated considering our results. The question which remains open and in which we will be interested is to know if the phase transition between the cubic form and the tetragonal form of $Rb_2KCrF_6$ and $Rb_2KGaF_6$ is achieved via the existence of intermediate phases, as can be predicted by the proposed model. One can imagine for example the existence of modulated phases what would imply the presence of structural frustration in the network.

## 5. Supporting information available

Further details of the crystal structure investigations can be obtained from the supporting information available from the Fachinformationszntrum Karlsruhe, 76344 Eggenstein-Leopoldshafen, Germany, (fax: (49) 7247-808-666; email: mailto:crysdata@fiz-karlsruhe.de) on quoting the depository numbers CSD-416605 ($Rb_2KGaF_6$ at 293 K), CSD-416606 ($Rb_2KGaF_6$ at 90 K) and CSD-416607 ($Rb_2KCrF_6$ at 90 K).

## References


[1] D. Babel, A. Tressaud, in: P. Hagenmuller (Ed.), Crystal Chemistry of Fluorides in Inorganic Solid Fluorides, Academic Press, New York, 1985, p. 143.

[2] I.N. Flerov, M.V. Gorev, K.S. Aleksandrov, A. Tressaud, J. Grannec, M. Couzi, Materials Science and Engineering—Review, Vol. 24, Elsevier, New York, 1998.

[3] D. Babel, R. Haegele, G. Pausewang, F. Wall, Mater. Res. Bull. 8 (1973) 1371.

[4] K.S. Aleksandrov, S.V. Misyul, Kristallografiya 26 (1981) 1074.

[5] R.D. Shannon, Acta Cryst. A 32 (1976) 751.

[6] A. Tressaud, S. Khairoun, J.P. Chaminade, M. Couzi, Phys. Stat. Sol. (a) 98 (1986) 417.

[7] J.M. Dance, J. Grannec, A. Tressaud, M. Moreno, Phys. Stat. Sol. (b) 173 (1992) 579.

[8] I. Flerov, A. Tressaud, K.S. Aleksendrov, M. Couzi, M.V. Gorev, J. Grannec, S.V. Melnikova, J.P. Chaminade, S.V. Misyul, V.N. Voronov, Ferroelectrics 124 (1991) 1309.

[9] I.N. Flerov, M.V. Gorev, A. Tressaud, J. Grannec, Ferroelectrics 217 (1998) 21.

[10] M.V. Gorev, I.N. Flerov, A. Tressaud, J. Grannec, Phys. Solid State 39 (1997) 1647.

[11] C. Marco de Lucas, F. Rodriguez, J.M. Dance, M. Moreno, A. Tressaud, J. Lumin. 48 & 49 (1991) 553.

[12] I.N. Flerov, M.V. Gorev, J. Grannec, A. Tressaud, J. Fluor. Chem. 116 (2002) 9.

[13] Oxford Diffraction 2003. CrysAlis Software Package, version 171. Oxford Diffraction sp. Zo. o, Wroclaw, Poland, Oxford Diffraction, 2003.

[14] V. Petricek, M. Dusek, L. Palatinus, Jana2000. Structure Determination Software Programs, Institute of Physics, Praha, Czech Republic, 2000.

[15] G. Siebert, R. Hoppe, Z. Anorg. Allg. Chem. 391 (1972) 117.

[16] A.M. Abakumov, M.D. Rossell, A.M. Alekseeva, S.Y. Vassilliev, S.N. Mudrezova, G.v. Tendeloo, E.V. Antipov, J. Solid State Chem. 179 (2006) 421–428.

[17] N.E. Brese, M. O' Keefe, Acta Crystallogr. B 47 (1991) 192–197.

[18] A.M. Glazer, Acta Crystallogr. B 28 (1972) 3384.

[19] K.S. Aleksandrov, Ferroelectrics 14 (1976) 801–805.

[20] P.M. Woodward, Acta Crystallogr. B 53 (1997) 32–43.

[21] C.J. Howard, H.T. Stokes, Acta Crystallogr. B 54 (1998) 782–789.

[22] P.M. Woodward, Acta Crystallogr. B 53 (1997) 44–66.

[23] B.G. Hyde, M. O'Keefe, Acta Crystallogr. A 29 (1973) 243–248.

[24] R.L. Withers, T.R. Welberry, F.J. Brink, L. Norén, J. Solid State Chem. 170 (2003) 211–220.